Journal of Ovonic Research Vol. 21, No. 6, November – December 2025, p. 819- 832

Enhanced spectral response and quantum efficiency in Cr_2O_3/ZnO/Si heterojunctions prepared via pulsed laser deposition

M. A. Ali [a,*] G. Z. Alwan [b], A. N. Abd [b], M. J. M. Ali [b,]
[a] *Applied Physics Department, College of Applied Science, University of Technology, 10066 Baghdad, Iraq*
[b] *Physics Department, College of Science, Mustansiriyah University, 10052 Baghdad, Iraq*

In this work, three Zinc oxide (ZnO) and Chromium (III) oxide (Cr_2O_3) based heterostructures Ag/ZnO/Si/Ag, Ag/Cr_2O_3/Si/Ag, and Ag/ZnO/Cr_2O_3/Si/Ag, were fabricated and characterized to evaluate their efficiency in solar cell and photodetector applications. All samples exhibited heterojunction behavior in I–V measurements conducted in both dark and illuminated conditions. The reverse current significantly improved under illumination, indicating effective electron-hole pair generation. This is particularly true for the Ag/ZnO/Cr_2O_3/Si/Ag binary structure, which recorded the highest forward current due to its low energy barrier and the synergistic effect between the two layers. Spectroscopically, in photodetector examinations, three main spectral peaks were observed: at ~350 nm (specific to ZnO), ~550 nm (specific to Cr_2O_3), and ~850 nm (specific to silicon). ZnO/Si showed a high response at ~350nm and ~850 nm, while Cr_2O3/Si showed a more pronounced peak at ~550 nm, ~850 nm, with a weak response in the ultraviolet range. ZnO/Cr_2O_3/Si combined the responses of both materials, showing improved performance in all ranges (UV-Vis-NIR). These results confirm that the ZnO/Cr_2O_3/Si binary structure offers unique optical and electronic integration, allowing for improved photosensitization efficiency in multiple spectral ranges without negatively affecting current stability in the dark. This structure also demonstrates its potential for integration into hybrid applications that combine efficient photoelectric conversion with high spectral response, enhancing its feasibility in sustainable energy systems and optical detection.

(Received September 30, 2025; Accepted December 11, 2025)

Keywords: Photodetector, Laser ablation, Chromium (III) oxide, Zinc dioxide, Solar cell

1. Introduction

Metal oxides are among the most attractive nanomaterials to researchers due to their wide band gaps, excellent chemical stability, and ease of structural modification, which enable them for several applications, especially in energy generation and optical sensing [1]. With an energy gap between 2.3 and 3.0 eV, Cr_2O_3 is unique among these oxides. Its exceptional absorption of visible light and resilience to extreme environmental conditions make it perfect for optical applications [2].

In contrast, ZnO is distinguished as a semiconductor with an energy gap of (~3.3) eV, making it a better choice in ultraviolet detectors, storage devices, and solar cells due to its high transparency in the visible range and its superior ability to transport electrons [3]. Studies have shown that integrating multiple oxides within a single nanostructure increases the efficiency of optical and photoelectric devices by reducing recombination, improving light absorption, and separating photovoltaic charges. In addition, the use of silicon (Si) as a cornerstone in the manufacture of optoelectronics, due to its ideal properties as a semiconductor and its good integration with oxide materials in nanostructures, makes it more widely used as a substrate and deposition base for these nanostructures and the possibility of good electrical conductivity within solar cell and photodetector applications [4, 5]. The use of Ag within these structures helps in electrical conductivity and increases light absorption due to the plasmon resonance

* Corresponding author: maryam.a.ali@uotechnology.edu.iq
https://doi.org/10.15251/JOR.2025.216.819

phenomenon [6]. Multilayers are among the most important materials in this field due to their efficiency in converting light energy into electrical energy and increasing the sensitivity of optical detection at various wavelengths. Among the prominent applications of these materials are solar cells, which rely on converting light into direct electrical current, and photodetectors, which are used to sense electromagnetic radiation and convert it into a measurable electrical signal, as shown in Fig. 1 [7, 8]. Despite the many studies that have addressed the synthesis of ZnO, Cr_2O_3 separately or in combination using traditional chemical methods such as thermal methods, chemical deposition, and sol gel, the laser ablation method in liquid provides an environment free of contaminants and produces highly pure nanoparticles characterized by tunable particle dimensions and distribution by adjusting the laser parameters. Previous research has shown that the particles produced by this technique are characterized by high efficiency compared to other techniques due to their lack of organic residues or surface contaminants. For example, Mutar, Z, S and Mutlak, F, A prepared ZnO particles by different techniques and deposited them on porous silicon substrates, showing efficiency of photonic absorption and energy transformation in photovoltaic applications [9]. Research conducted by Chatzigiannakis, G. *et al*. proved the effect of laser-prepared microstructure on the effectiveness of ZnO and Si solar cells, showing improved response across a wide spectrum [10]. In addition, a study by Rabia, M., *et al*., which dealt with the preparation of a thin film of Cr_2O_3-Cr $(OH)_3$-Polypyrrole/Polypyrrole and its use in photodetectors and solar cells, showed excellent photo response results and good energy conversion efficiency [11]. In this research, three nanostructures were prepared on a silicon substrate. Ag/ZnO/Si/Ag, Ag/Cr_2O_3/Si/Ag, Ag/ZnO/Cr_2O_3/Si/Ag. The integration of Cr_2O_3 and ZnO on a silicon substrate enhances light absorption across a broad spectrum and increases charge separation efficiency. The goal of this work is to investigate these nanostructures in two complementary practical applications: Solar cells: By analyzing the current-voltage (I–V) characteristics under forward and reverse biases for each structure, we evaluate the dual behavior and photovoltaic potential and photodetectors: Through quantification of specific detectivity (D*), responsivity (R) and external quantitative efficiency (EQE), we determine the spectral sensitivity and photon-to-electrical conversion efficiency. Also, after studying their structural and optical properties and knowing the surface topography to make them suitable for increasing the absorption spectrum in the ultraviolet and visible regions, which in turn increases the spectral response and improves the electrical properties of silicon detectors.

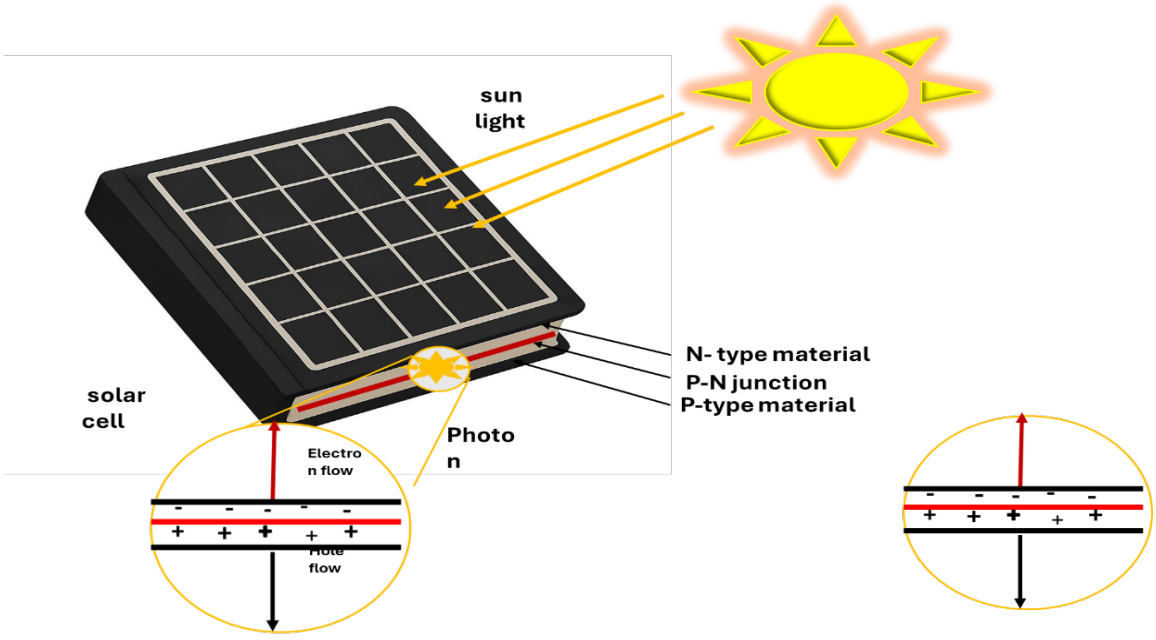

Fig. 1. Basic diagram of Photovoltaic solar cell.

2. Experimental parts

2.1. Preparation of (Cr_2O_3 and ZnO) NPs using the laser ablation method.

The synthesis of Cr_2O_3 and ZnO NPs by pulsed laser ablation of a high-grade composition for Cr as well as Zn target in deionized water (DI). A 5-ton hydraulic press was utilized for a duration of 20 min; a mixture of 5 g high-purity Cr and Zn powder was placed inside a hydraulic press mold to form metal pellets with a diameter of 1.5 cm. The next procedure was to place a (Cr and Zn) target in a glass vessel with 50 mL of (DI) water, and focus a laser beam on a (Cr and Zn) target. The type of laser beam was Nd: YAG with a wavelength of 1064 nm shone on it. The target ablation procedure was performed using a laser beam with 600 pulses, a constant energy of 500 mJ per pulse, and a frequency of 8 Hz.as seen in Fig. 2.

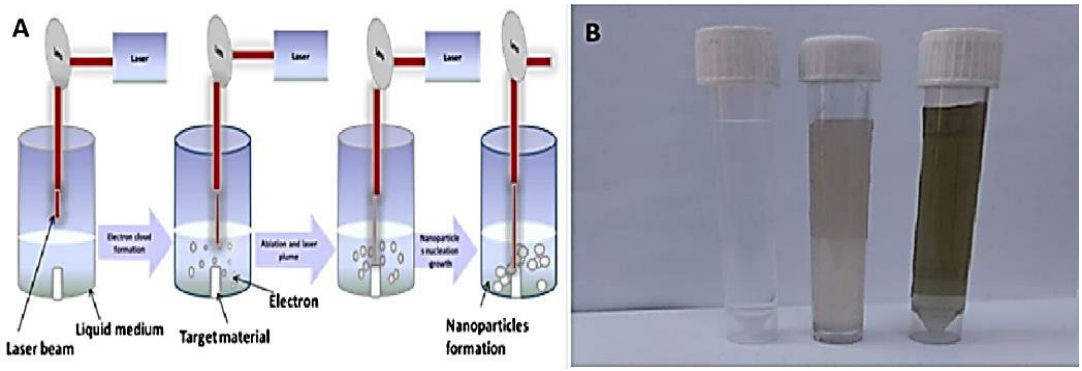

Fig. 2. (A) Sketch of the laser ablation process. (B) The preparation of ZnO and Cr_2O_3: from left to right are (DI) water, ZnO and Cr_2O_3, respectively.

2.2. Fabrication of a photodetector by the drop casting method.

A 1.5 × 1.5 cm polished silicon (Si) substrate was processed using an ultrasonic bath containing a mixture of ethanol and acetone for 20 minutes. This was followed by drying the substrate by heating at 50 °C. After cleaning, a micropipette was used to drop a specific amount of the pre-prepared nanoparticle solution (ZnO and Cr_2O_3) onto the substrate surface, ranging from (20 to 50) mL. The sample underwent gradual drying on a heated plate at (50 ± 10) °C to ensure the formation of a cohesive layer and uniform nanoparticle distribution. Subsequently, silver paste was applied to both ends of the deposition zone to create electrodes that ensure effective contact between the active material and the external circuit. The silver paste was then fixed using a 100 W tungsten lamp for 10 minutes to ensure good adhesion between the electrodes and the substrate surface. The steps of this process are illustrated in Fig. 3.

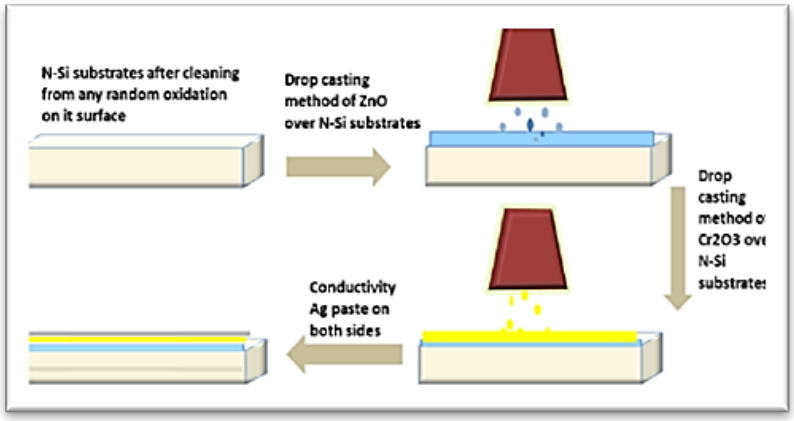

Fig.3. Schematics demonstrating the fabrication process of the Ag/ZnO/Cr_2O_3/Si/Ag heterojunction.

2.3. Description of the electrical circuit installation.

To measure the current and voltage, a Keithley-616 digital multimeter, a Tektronics CDM 250 millimeter, and a Farnel LT30/2 dual power supply with a voltage range of 0–5 V were used. The forward current was recorded when a positive voltage was applied across the contact point of the aluminum metal with the nanostructure layer relative to the aluminum electrode on the crystalline silicon substrate.

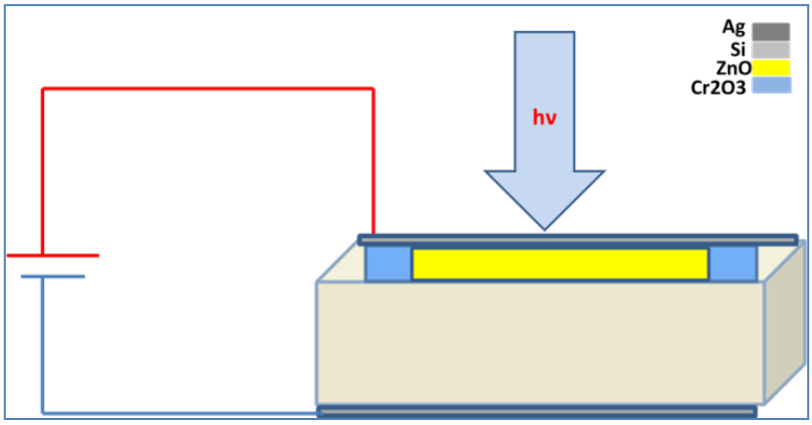

Fig.4. Electrical circuit installation.

3. Results and discussion.

X-Ray diffraction analysis of samples Cr_2O_3 and ZnO was performed using the SHIMADZU XRD-6000 apparatus manufactured in Japan, relying on CuKα radiation with a wavelength of 1.5406 Å. As shown in Fig. 5, the emergence of a broad dominant peak at 24.6°, corresponding to the (012) plane, is attributed to the Escolite phase (α-Cr_2O_3) of the Quarundum system according to the (JCPDS card No. 1308-38-9) [12], with the absence of other sharp peaks. The crystallite size was calculated using the Scherrer equation [13], where the peak width at mid-intensity (FHWM) was 8.3°, resulting in a crystallite size of approximately 1.04 nm. This very small size indicates that the material has a semi-amorphous structure or very small nanocrystals. This behavior is highly expected in materials prepared by physical methods such as laser ablation [14]. These results confirm the effectiveness of the preparation method in producing nanomaterials with very small crystallite size. The XRD analysis of the ZnO sample revealed a sharp and high peak. The most intense peak appeared at 2θ = 31.8° and 36.4° corresponding to the (100) and (101) crystal planes respectively, which is the most distinct plane in ZnO (JCPDS card No. 19–1458) [15]. The XRD pattern revealed extra peaks located at 2θ = 34.5°, 47.8°, 56.7°, 68.3°, and 58.0°, corresponding to the (002), (102), (110), (103), and (112) planes, respectively, demonstrating that the sample exhibits crystallization within the hexagonal wurtzite structure [16]. The mean crystallite size was calculated to be approximately 6.45 nm for ZnO. Table 1 summarizes the XRD data and calculated parameters for ZnO and Cr_2O_3.

$$D = \frac{0.94\lambda}{\beta\cos\theta} \qquad (1)$$

Where χ is the wavelength of the X-ray (1.5406 Å) for CuKα radiation, β is the full width at half maximum, and Θ is the peak position.

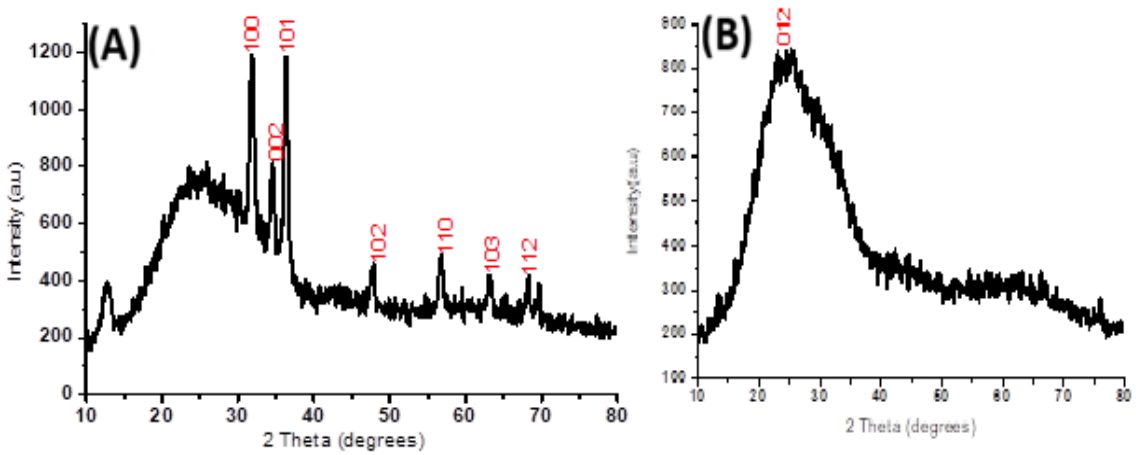

Fig.5. X-ray diffraction pattern of the (A) ZnO thin film. (B) Cr_2O_3 thin film.

Table 1. XRD results and estimated parameters for $Cr_2O_3$and ZnO thin films.

Samples	2θ (deg)	FWHM (deg)	d_{hkl} Exp.(Å)	D (nm)	hkl
Cr_2O_3	24.6º	8.3	3.6159	1.04	012
ZnO	31.8º	1.42	5.8117	5.8	100
	36.4º	1.17	2.4663	7.1	101

Absorption spectra of both Cr_2O_3 and ZnO compounds were analyzed using UV-Vis spectroscopy with a (DU-8800D) spectrophotometer (China) in the wavelength range of (190–1100) nm, as shown in Fig. 6. This analysis was used to study the optical response of each material and determine its band gaps. The spectrum showed a sharp absorption edge at about 200 nm for Cr_2O_3 and 250 nm for ZnO. The optical energy gap was calculated using the Tauc plot and found to be about 3.2 eV and 3.85 eV for Cr_2O_3 and ZnO, respectively [17]. These results indicate that the material has a wide energy gap, which is consistent with its nanoscale nature and phase variations.

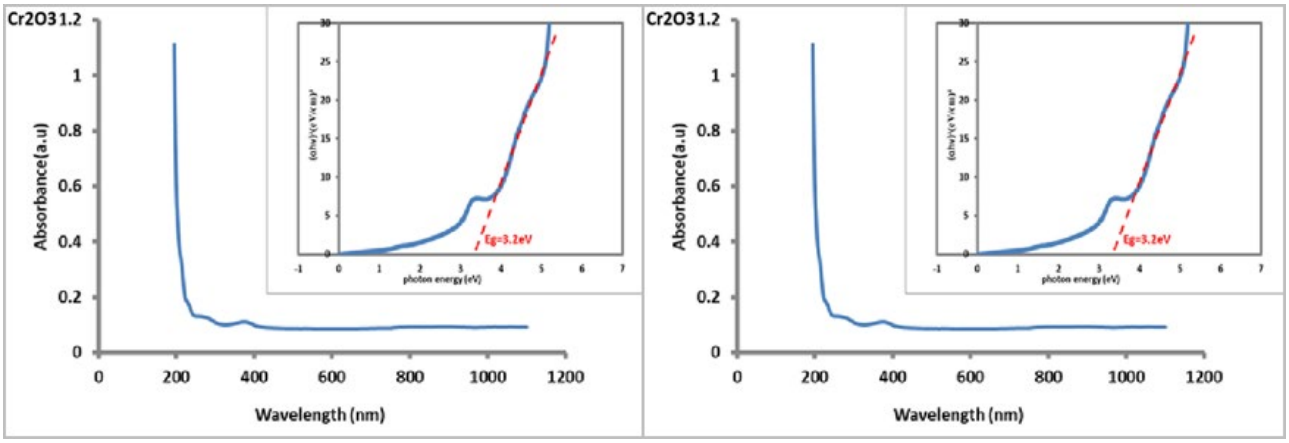

Fig. 6. UV-Vis absorption spectra and estimated energy band gap of ZnO and Cr_2O_3 NPs.

FTIR spectroscopy (ATR-FTIR, ALPHA-BRUKER) was used to analyze the nature of chemical bonds and to identify the functional groups present in Cr_2O_3 and ZnO compounds, as shown in Fig. 7. The formation of the Cr_2O_3 compound was verified by the appearance of characteristic absorption peaks at 464, 526, and 636 cm^{-1}, which are due to the stretching vibrations of the Cr-O bond [18]. Moreover, an absorption peak at 907 cm^{-1} was observed linked to the (Cr-O-H) bending [18]. It is due to the hydroxyl group being linked to Chromium. The peak at 1116 cm^{-1} due to - Co_3^{-2} indicates the presence of traces of impurities or surface bonds. The intense peak at 1384 cm^{-1} returns to (C-H) bending due to organic impurities [19]. The peaks at 1650 cm^{-1} and 3470 cm^{-1} are related to (H-O-H) bending and (O-H) stretching [20]. The spectral peak at 650 cm^{-1} represents the stretching vibration mode of the (Zn-O) bond, confirming the formation of ZnO [21], The peak at 878 cm^{-1} due to (Zn-OH) surface impurities [22]. A peak also appeared at 1469 cm^{-1}, resulting from surface carbonates ($-CO_3$) [23]. In addition, peaks at 1626 cm^{-1} and 3437 cm^{-1} are associated with (H-O-H) bending and (O-H) stretching [23]. Lastly, an intense peak was detected at 2922 cm^{-1}, revealing the presence of surface adsorption of organic molecules or solvent residues. which is attributed to (C-H) stretching [22].

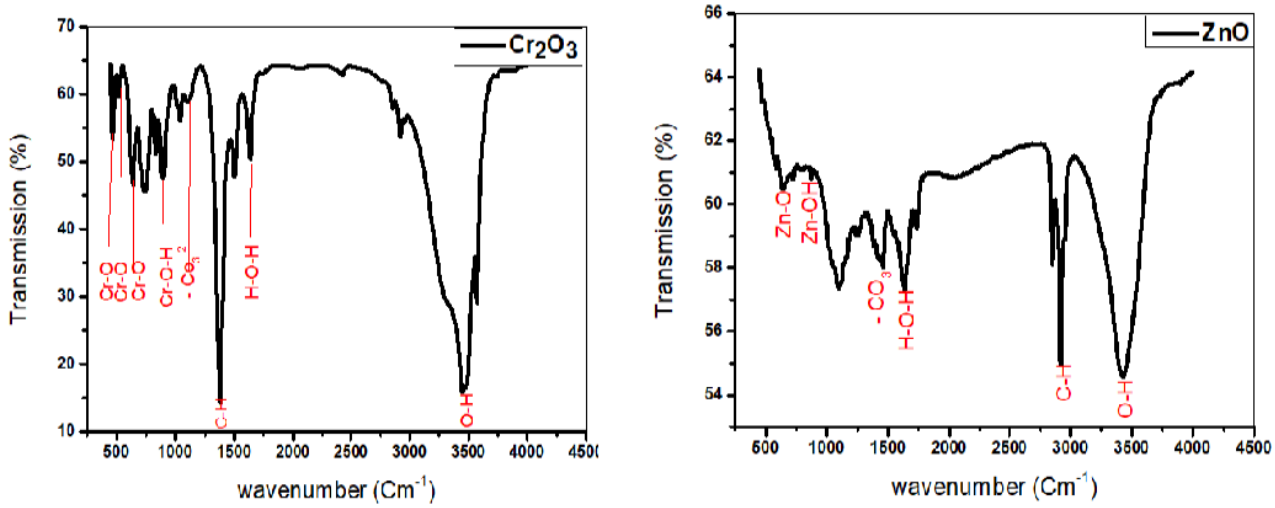

Fig. 7. FTIR spectrum for Cr_2O_3 and ZnO thin films.

Atomic energy microscopy (AFM) analysis of Cr_2O_3 and ZnO thin films using a Digital Instruments system (Nano scope III and Dimension) was performed to determine the surface structure and morphological properties with nanoscale resolution, as shown in Fig. 8 and Fig. 9. The sample was imaged over an area of 2.0 × 2.0 µm. The three-dimensional image showed a homogeneous distribution of thin film with a clear absence of large agglomerates, reflecting the efficient preparation of the material using the laser ablation in liquid (LAL) technique. In the Cr_2O_3 sample, the average particle height was 13.39 nm with a root mean square RMS = 807 pm, and the accompanying histogram showed that most particles had heights ranging from 17 to 19 nm, with a significant concentration at less than 18 nm. As for ZnO, the average particle height was 2.81 nm with RMS = 710 pm, most of the particles had heights ranging from 13 to 15 nm, with a significant concentration at less than 15 nm. This indicates a relatively smooth surface and a fine nanostructure; the prepared particles are very small and exhibit distinct nanoscale properties in both materials. The results of this study indicate that some particles might be single crystals or small clusters of crystals, which is in line with the crystal size according to what (XRD) analysis reveals. The band gap, which was identified by UV-Vis scanning and clearly shows a quantum confinement effect, also widens because of the small size.

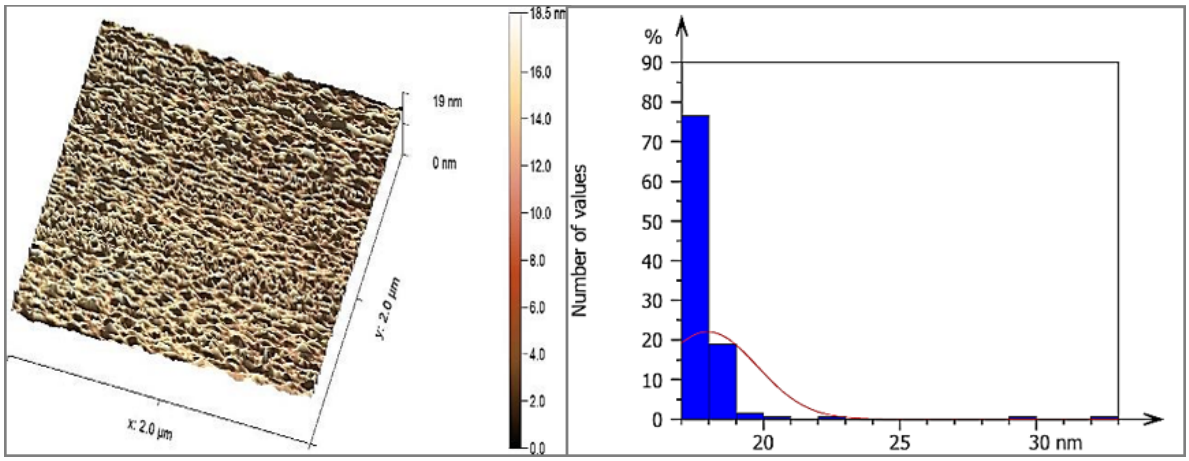

Fig. 8. AFM of Cr_2O_3 thin film.

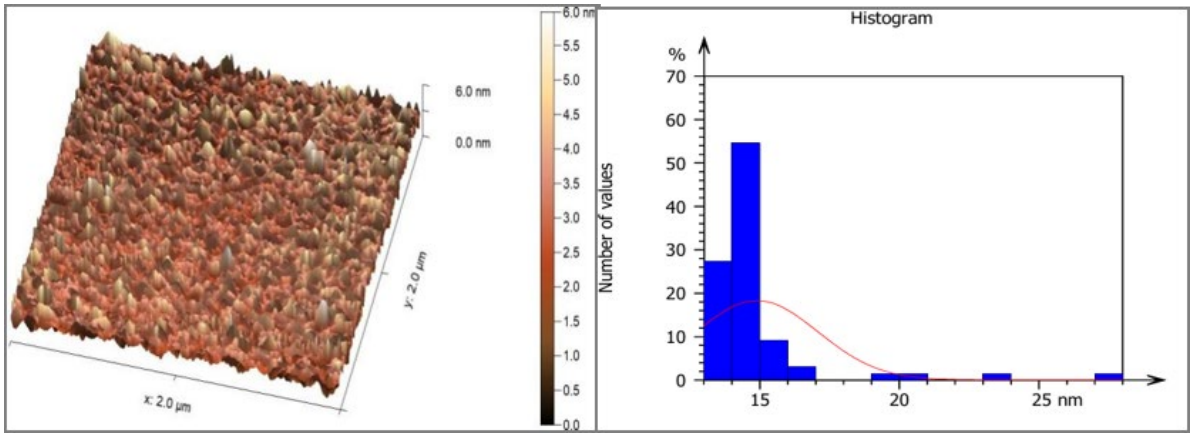

Fig. 9. AFM of ZnO thin film.

The FESEM images used (MIRA3 TESCAN) at 135X and 70X magnifications, shown in Fig. (10a) for the Cr_2O_3 sample, showed semi-spherical particles with a close distribution and fine nanocluster formation, indicating uniform growth without large agglomerates. A typical particle was measured and found to be approximately 28.09 nm. This is consistent with the XRD scan, which showed a crystallite size of approximately 1.04 nm, indicating that the particles observed in the FESEM scan consist of multiple nanocrystalline aggregates. The FESEM scan in Fig. (10b) for the ZnO sample showed semi-spherical particles with an irregular distribution, fine nanocluster formation, and an absence of large agglomerates, the typical particle size was approximately 53.84 nm.

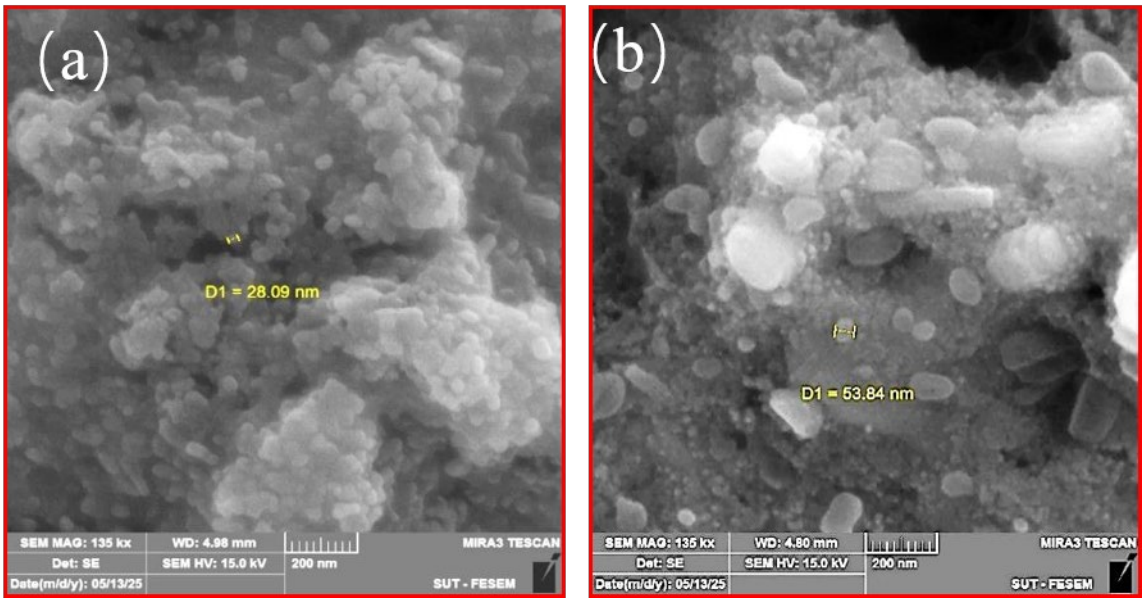

Fig. 10. FESEM of Cr_2O_3 and ZnO thin films (left to right).

The electrical behavior of the Ag/ZnO/Si/Ag heterojunction was investigated through the measurement of the (current -voltage) curves under non-illuminated and illumination conditions as seen in Fig. 11. The I–V results showed the heterojunction behavior, where the reverse current remained low and the forward current increased exponentially with voltage, indicating the dominance of the diffusion current in the device [24]. When the sample was exposed to light, a significant increase from 20 µA to 130 µA at 5 V in the reverse current was observed under the reverse voltage, reflecting the high efficiency in converting light energy into electrical current. This performance is linked to the expansion of the depletion region and the increased photoinduced electron-hole pair generation, in addition to the regular nanostructure of the ZnO layer, which enhances photon absorption and improves the photovoltaic performance of the device [25, 26].

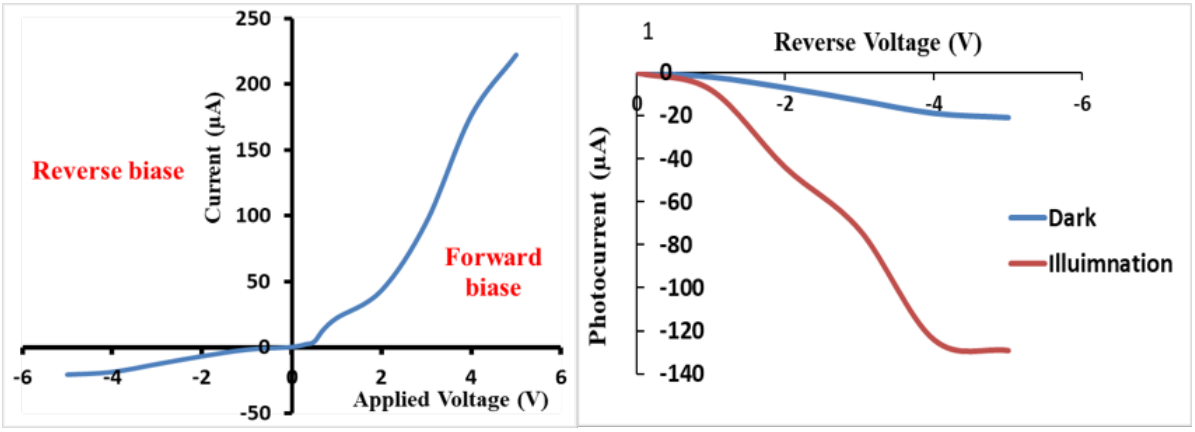

Fig. 11. (I–V) in the dark characteristics' curves and Photocurrent in (bright-dark) under the effect of reverse bias of Ag/ZnO/Si/Ag.

When the ZnO layer was replaced by Cr_2O_3 in the Ag/Cr_2O_3/Si/Ag structure as shown in Fig. 12. The (I–V) curves in the dark showed almost constant reverse current over the voltage range of (–1 to –5) V, with a slightly higher forward current value than that recorded for ZnO, indicating a lower energy barrier and increased in the Cr_2O_3/Si junction [25, 26]. However, when the sample underwent illumination, a clear increase in the reverse current

was also observed. These results indicate that both ZnO and Cr_2O_3 can be used as active layers in heterojunction solar cells, with the possibility of achieving higher performance using Cr_2O_3 [27].

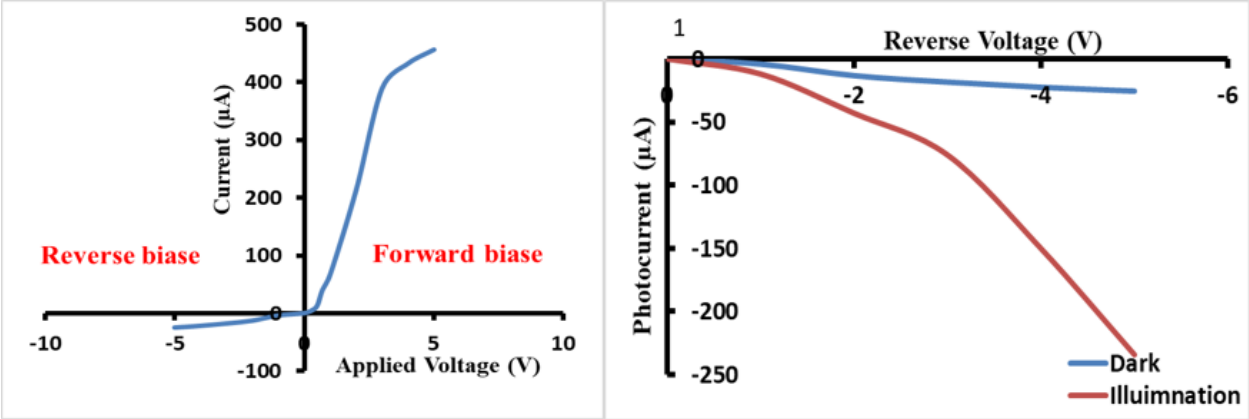

Fig. 12. (I–V) in the dark characteristics' curves and Photocurrent in (bright-dark) under the effect of reverse bias of Ag/Cr_2O_3/Si/Ag.

In Fig. 13, we notice that when Cr_2O_3 was added to ZnO in Ag/ZnO/Cr_2O_3/Si/Ag compound, the reverse current in the dark remained almost constant, as it was in the ZnO-only sample, and no additional increase or leakage occurred when Cr_2O_3 was added. This indicates that Cr_2O_3 did not create additional leakage paths or surface defects, and that this compound still maintains the good barrier properties between the ZnO/Cr_2O_3 layer and the silicon. As for the forward current, we notice a significant increase of approximately 490 µA. This is due to reducing the energy barrier at the heterojunction due to the presence of two different layers of Cr_2O_3 and ZnO and the synergistic effect between them, which enhances the overall conductivity of the active layer, as well as increasing the density of surface states or improving contact between the layers [28,29]. The significant increase in reverse current, reaching 240 µA when exposed to light, indicates that the cell has become more sensitive to light and is more capable of generating electron-hole pairs upon absorbing photons [31–32]. These results enhance the performance of the solar cell and confirm the effectiveness of the bilayer in improving light absorption and charge separation without negatively affecting the reverse current in the dark.

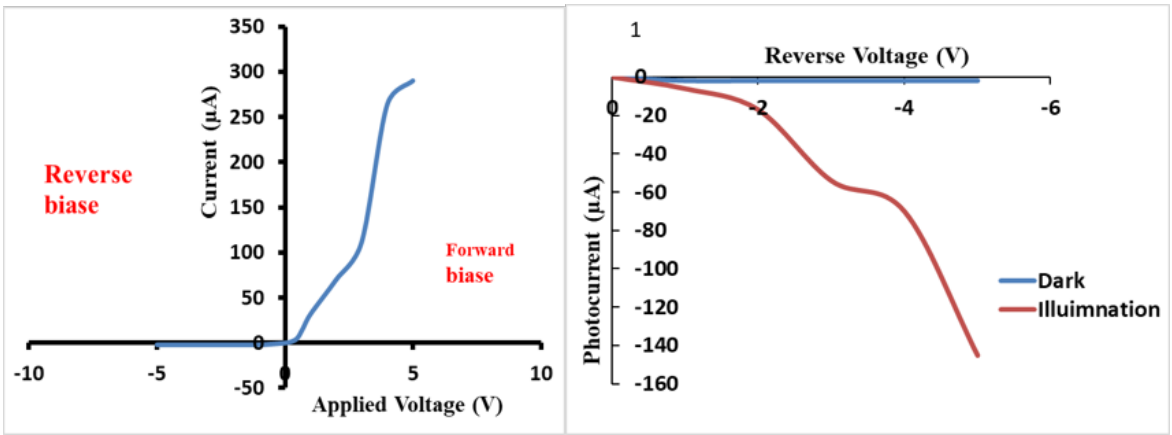

Fig. 13. (I–V) in the dark characteristics' curves and Photocurrent in (bright-dark) under the effect of reverse bias of Ag/ZnO/Cr_2O_3/Si/Ag heterojunction.

The D*, R and EQE as a function of wavelength in the range of (200–1000) nm were studied. These parameters were derived based on the following equation [30]:

$$R = \frac{I_{ph} - I_d}{PA} \quad (2)$$

$$D* = \frac{R}{\sqrt{\frac{2eI_d}{A}}} \quad (3)$$

$$EQE = R\frac{hc}{e\lambda} \quad (4)$$

where I_{ph} is photocurrent, I_d is dark current, P is power density of incident light, A is effective irradiation area, e is electron charge, h is Planck's constant, c is speed of light, and λ is wavelength of the incident light. The results revealed distinct optical behaviors that depend on the type of active nanolayer. The performance of the Ag/ZnO/Si/Ag detector in Fig. 14 shows that R, D* and EQE exhibit a sharp peak at ~350 nm resulting from the strong UV absorption by the ZnO thin film, which has a bandgap of 3.85 eV. Another sharp peak for both R and D* appears at ~830 nm, which is attributed to the contribution of the silicon substrate, which has a bandgap of 1.1 eV, allowing for NIR absorption. The EQE at this wavelength is less sharp, resulting from losses in the photon-to-current conversion process, either due to recombination or collection in this spectral region. A rapid decline in response is observed after 400 nm, indicating poor sensitivity in the visible light range.

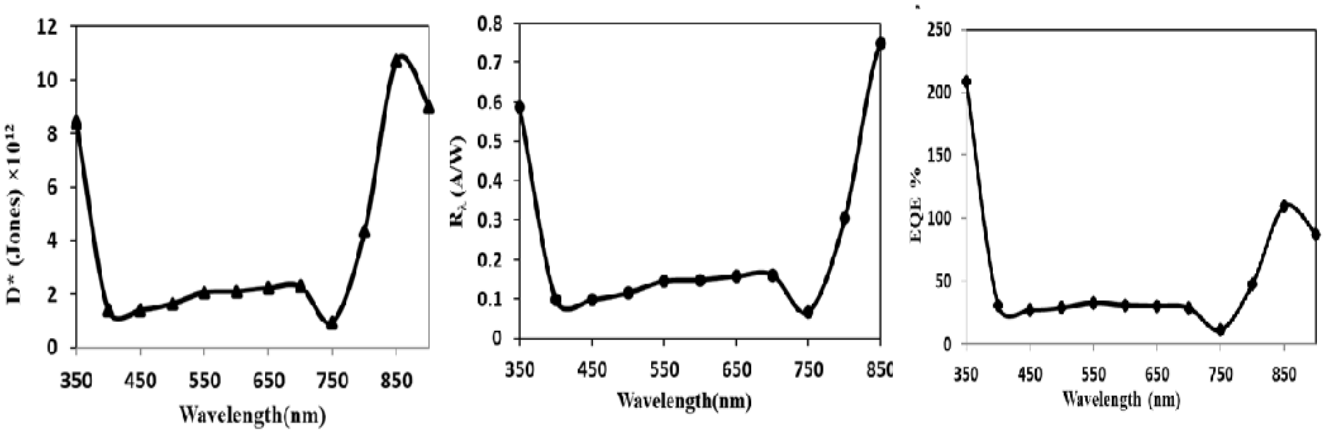

Fig. 14. R, D and EQE of Ag/ZnO/Si/Ag Photoelectric.*

Fig. 15 shows the photoelectron spectrum of Ag/Cr_2O_3/Si/Ag detector. There are three main peaks in R, D*, and EQE with different intensities. A slight increase in all three coefficients was observed at a wavelength of ~350 nm and a sharp peak at ~550 nm, indicating a high ability of the active layer to absorb photons in the visible range. Even though the Cr_2O_3 energy gap is 3.2 eV, its absorption was weak in the UV region and a sharp peak in the visible spectrum. In addition to the structural effect between Cr_2O_3 and Si within the junction interface, this may be interpreted by the presence of intermediate energy levels or indirect transitions that enable effective absorption in the visible range and the low charge collection efficiency in the UV region caused by surface recombination [33,34], which may create new absorption bands outside the range expected from the theoretical energy gap. The detector shows a remarkable response at ~850 nm, where two clear peaks appear in D* and R, while the EQE peak is less sharp, reflecting silicon absorption in the near-infrared (NIR) range.

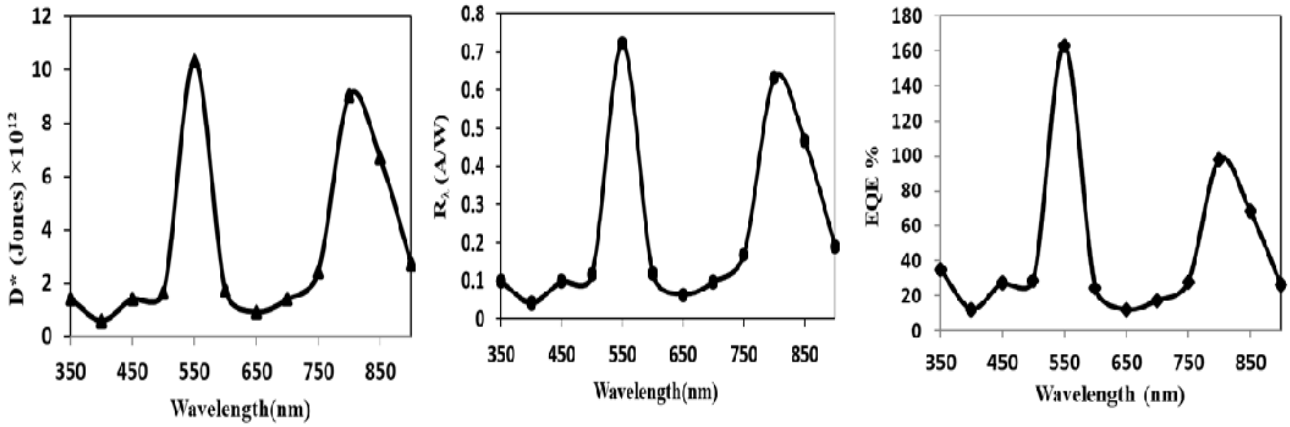

Fig. 15. R, D and EQE of Ag/Cr_2O_3/Si/Ag Photoelectric.*

Fig. 16 shows the photoelectron spectrum of the Ag/ZnO/Cr_2O_3/Si/Ag detector. The multiband spectral response is a result of the combined synergy between Cr_2O_3 and ZnO. At ~350 nm in the UV range, a more intense response was observed than at Ag/Cr_2O_3/Si/Ag detector and less than at Ag/ZnO/Si/Ag detector at D*, R, and EQE. This indicates that both layers share photon absorption in this region. However, the presence of Cr2O3 contributes to a modification of the energy structure and reduces the relative effectiveness of ZnO, possibly because of internal barriers or internal potential redistribution. At wavelengths of ~550 nm, peaks almost identical to those recorded for the Ag/Cr_2O_3/Si/Ag detector were observed, indicating that the response in this region is dominated by Cr_2O_3 absorption, supporting the hypothesis that the chromium substrate remains active in the visible range even in the presence of ZnO. In the near-infrared (NIR) range at ~850 nm, the specific response and sensitivity (R and D*) were higher than Ag/Cr_2O_3/Si/Ag detector and lower than Ag/ZnO/Si/Ag detector, while the EQE remined identical for all samples, reflecting a significant improvement in silicon absorption due to the double-layered arrangement, which provides a better path for charge collection and reduces charge loss at the interface. The integrated nanostructure also helped enhance absorption across layers and efficient electron transport, which enhances the performance of detectors and solar cells without causing leakage or loss of efficiency.

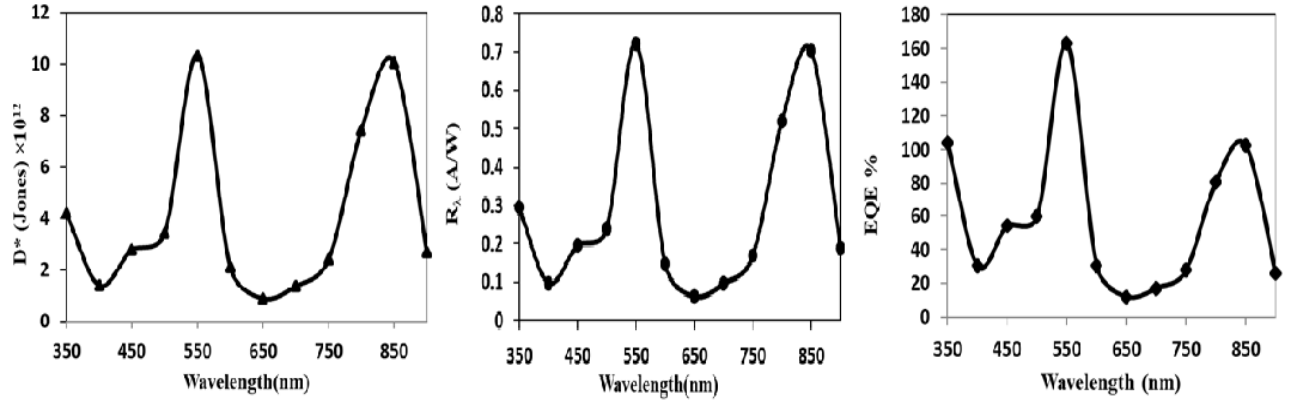

Fig. 16. R, D and EQE of Ag/ZnO/Cr_2O_3/Si/Ag Photoelectric.*

4. Conclusions

In this research, the performance of three thin films based on ZnO and Cr_2O_3 were fabricated and evaluated by laser ablation technique. Three compounds named Ag/ZnO/Si/Ag, Ag/Cr_2O_3/Si/Ag, Ag/ZnO/Cr_2O_3/Si/Ag heterojunctions. These investigations were using various techniques such as FTIR, XRD, FESEM, AFM and UV-Vis to study encompassed analysis of structure, morphology and optical properties, as well as evaluation of electrical properties using by R, D* and EQE. The photodetectors and solar cells fabricated from these three compounds showed identical and correlated behavior at the spectral and photoelectric levels, where it was observed that the Ag/ZnO/Cr_2O_3/Si/Ag detector is the most superior and efficient compared to the other detectors. This behavior is caused by its broad spectral response across a wide wavelength range (UV-Vis and NIR) with a significant enhancement in detection sensitivity and photoelectric conversion efficiency. There is also a significant increase in the performance of the solar cell, both in terms of forward current and reverse current response under illumination, while maintaining a constant reverse current in the dark and reducing electrical losses. This is due to the synergistic effect between ZnO and Cr_2O_3, which enhances multiband absorption. Although Ag/ZnO/Si/Ag detector contributed to highly effective absorption of (UV and NIR) range, while Cr_2O_3 in Ag/Cr_2O_3/Si/Ag detector improved the performance of optical detectors in the (Vis and NIR) range. These developments represent a step towards creating a new generation of high-performance optical detectors, with potential deployment in photonic sensing devices suitable for environmental analysis and high-performance photonic platforms.

Availability of Data and Materials

The data and materials used in this study are available from the corresponding author upon reasonable request

Author Contributions

A.N. Abd performed the experimental work**;** M. A. Ali supervised the study and served as the corresponding author; M. J. Ali reviewed and edited the manuscript; G. Z. Alwan drafted the manuscript.

All authors contributed to the critical revision of the manuscript for important intellectual content.
All authors read and approved of the final manuscript.
All authors have participated sufficiently in the work and agreed to be accountable for all aspects of the work.

Acknowledgment

We would like to express our sincere gratitude to everyone who supported us during the preparation of this manuscript. We also thank the peer reviewers for their valuable comments and constructive suggestions, which helped improve the quality of this work**.**

Funding

The research received no external funding

Conflict of Interest

The authors declare no conflict of interest

References

[1]B. Ding, C. Yang, Y. Chen, W.P. Shao, F. Yang, C. Zhang, Z. Wang, Y. Liu, Y. Cao, Y. Zhu, X. Bao, ChemCatChem **16**(23), e202401421 (2024). https://doi.org/10.1002/cctc.202401421
[2] S. Zahra, W. A. A. Syed, N. Rafiq, W. H. Shah, Z. Iqbal, Protection of Metals and Physical Chemistry of Surfaces **57**(2), 321 (2021). https://doi.org/10.1134/S2070205121010238

[3] P. Kumari, A. Srivastava, R. K. Sharma, D. Sharma, S. K. Srivastava, Nanomaterials for Innovative Energy Systems and Devices, Springer, Singapore (2022).
[4] H. Rai, K. R. B. Singh, S. S. Pandey, A. Natarajan, Journal of Molecular Structure **1316**, 138994 (2024). https://doi.org/10.1016/j.molstruc.2024.138994
[5] R. Savkina, O. Smirnov, S. Mulenko, 2022 IEEE 41st International Conference on Electronics and Nanotechnology (ELNANO), IEEE, Kyiv (2022). https://doi.org/10.1109/ELNANO54634.2022.9786842
[6] S.J. Ko, H. Choi, W. Lee, T. Kim, B. R. Lee, J.W. Jung, J.R. Jeong, M. H. Song, J. C. Lee, H. Y. Woo, Energy & Environmental Science **6**(6), 1949 (2013). https://doi.org/10.1039/C3EE40575A
[7] S. L. Pyshkin, J. Ballato, Optoelectronics - Materials and Devices, InTech, London (2015). https://doi.org/10.5772/59334
[8] K. Shekhawat, P. Prajapat, G. Gupta, D. Negi, R. Shyam, M. Gupta, S. R. Nelamarri, Optical Materials **154**, 115654 (2024). https://doi.org/10.1016/j.optmat.2024.115654
[9] Z. S. Mutar, F. A.H. Mutlak, Journal of Optics **54**(1), 1 (2025). https://doi.org/10.1007/s12596-024-01687-2
[10] G. Chatzigiannakis, A. Jaros, R. Leturcq, J. Jungclaus, T. Voss, S. Gardelis, M. Kandyla, ACS Applied Electronic Materials **2**(10), 2819 (2020). https://doi.org/10.1021/acsaelm.0c00630
[11] M. Rabia, A. B. G. Trabelsi, A. M. Elsayed, F. H. Alkallas, Coatings **13**(7), 1240 (2023). https://doi.org/10.3390/coatings13071240
[12] A. Kantor, I. Kantor, M. Merlini, K. Glazyrin, C. Prescher, M. Hanfland, L. Dubrovinsky, American Mineralogist **97**(10), 1764 (2012). https://doi.org/10.2138/am.2012.4103
[13] W. J. Aziz, G. Z. Alwan, R. S. Sabry, AIP Conference Proceedings **2922, 040001 (2024)**. https://doi.org/10.1063/5.0196789
[14] M. H. Wu, R. Mu, A. Ueda, D. O. Henderson, MRS Online Proceedings Library (OPL) **780**, Y3.2 (2003). https://doi.org/10.1557/PROC-780-Y3.2
[15] T. Vu Anh, T. A. T. Pham, V. H. Mac, T. H. Nguyen, Journal of Analytical Methods in Chemistry **2021**, 5533734 (2021). https://doi.org/10.1155/2021/5533734
[16] A. Mohammada, H. A. AlJafa, H. S. Ahmeda, M. Mohammedb, Z. Khodairc, Journal of Ovonic Research **18**(3), 443 (2022).
[17] D. Parajuli, S. Dangi, B. R. Sharma, N. L. Shah, D. KC, Bibechana **20**(2), 113 (2023). https://doi.org/10.3126/bibechana.v20i1.47412
[18] F. H. Mohammed, H. M. Mikhlif, Iraqi Journal of Physics **19**(3), 79 (2021).
[19] J. M. Guyt, M. Van Eesbeek, G. Van Papendrecht, Optical System Contamination: Effects, Measurements, and Control VII, SPIE, Seattle (2002). https://doi.org/10.1117/12.453524
[20] L. Li, Z.F. Yan, G. Q. Lu, Z. H. Zhu, The Journal of Physical Chemistry B **110**(1), 178 (2006). https://doi.org/10.1021/jp0545069
[21] Z.F. Wu, S.J. Li, Chinese Journal of Spectroscopy Laboratory **29**(4), 2172 (2012).
[22] A. A. Tsyganenko, J. Lamotte, J. Saussey, J. C. Lavalley, Journal of the Chemical Society, Faraday Transactions 1: Physical Chemistry in Condensed Phases **85**(8), 2397 (1989). https://doi.org/10.1039/F19898502397
[23] F. Boccuzzi, C. Morterra, R. Scala, A. Zecchina, Journal of the Chemical Society, Faraday Transactions 2: Molecular and Chemical Physics **77**(11), 2059 (1981). https://doi.org/10.1039/F29817702059
[24] K. Abe, T. Komiyama, Y. Chonan, H. Yamaguchi, T. Aoyama, physica status solidi (c) **9**(6), 1352 (2012). https://doi.org/10.1002/pssc.201100676
[25] M. Vetrivel, A. Jagadeeshwaran, B. Sangeetha, Journal of Ovonic Research **20**(6), 841 (2024). https://doi.org/10.15251/JOR.2024.206.841
[26] W.Y. Zhang, X.P. Wang, L.J. Song, B.X. Liu, Z.X. Fu, Acta Physica Sinica **57**(7), 4471 (2008). https://doi.org/10.7498/aps.57.4471
[27] S. Kansal, J. Halder, D. Mandal, R. Rahul, S. Priya, P. De, V. Sharma, A. K. Srivastava, T. Singh, A. Chandra, Materials Science and Engineering: B **293**, 116438 (2023). https://doi.org/10.1016/j.mseb.2023.116438
[28] A. Razzaq, M. Zafar, T. Saif, J. Y. Lee, J. K. Park, W. Y. Kim, Journal of Nanoscience and Nanotechnology **21**(7), 3800 (2021). https://doi.org/10.1166/jnn.2021.19234
[29] D. Smazna, N. Wolff, S. Shree, F. Schütt, Y. K. Mishra, L. Kienle, R. Adelung, 2017 IEEE 7th International Conference on Nanomaterials: Applications and Properties (NAP), IEEE, Odessa (2017).

https://doi.org/10.1109/NAP.2017.8190199
[30] S. Fomanyuk, A. Ishchenko, M. K.L. T., pubs.aip.org **2024**(1), 012003 (2024). https://doi.org/10.1063/5.0178901
[31] M. A. Ali, G. Z. Alwan, Digest Journal of Nanomaterials and Biostructures **20**(3), 769-780 (2025). https://doi.org/10.15251/djnb.2025.203.769
[32] A. B. F. Martinson, J. E. McGarrah, M. O. K. Parpia, J. T. Hupp, Physical Chemistry Chemical Physics **8**(38), 4655 (2006). https://doi.org/10.1039/B610566A
[33] A. I. Mostovoi, V. V. Brus, P. D. Maryanchuk, Semiconductors **48**(9), 1174 (2014). https://doi.org/10.1134/S1063782614090164
[34] J. Hu, X. Zhao, W. Chen, Z. Chen, ACS Omega **3**(10), 14973 (2018). https://doi.org/10.1021/acsomega.8b01195